Published in final edited form as:
*Biomater Sci*. 2014 May 1; 2(5): 655–665. doi:10.1039/C3BM60274E.

# Hyaluronic acid hydrogel stiffness and oxygen tension affect cancer cell fate and endothelial sprouting

**Yu-I Shen**[1], **Hasan E. Abaci**[1], **Yoni Krupsi**[1], **Lien-Chun Weng**[1], **Jason A. Burdick**[2], and **Sharon Gerecht**[1,*]

[1]Department of Chemical and Biomolecular Engineering, Johns Hopkins Physical Sciences-Oncology Center and Institute for NanoBioTechnology, Johns Hopkins University, Baltimore, MD 21218.

[2]Department of Bioengineering, University of Pennsylvania, Philadelphia, PA 19104 USA.

## Abstract

Three-dimensional (3D) tissue culture models may recapitulate aspects of the tumorigenic microenvironment *in vivo*, enabling the study of cancer progression *in vitro*. Both hypoxia and matrix stiffness are known to regulate tumor growth. Using a modular culture system employing an acrylated hyaluronic acid (AHA) hydrogel, three hydrogel matrices with distinctive degrees of viscoelasticity — soft (78±16 Pa), medium (309± 57 Pa), and stiff (596± 73 Pa) — were generated using the same concentration of adhesion ligands. Oxygen levels within the hydrogel in atmospheric (21 %), hypoxic (5 %), and severely hypoxic (1 %) conditions were assessed with a mathematical model. HT1080 fibrosarcoma cells, encapsulated within the AHA hydrogels in high densities, generated nonuniform oxygen distributions, while lower cell densities resulted in more uniform oxygen distributions in the atmospheric and hypoxic environments. When we examined how varying viscoelasticity in atmospheric and hypoxic environments affects cell cycles and the expression of *BNIP3* and *BNIP3L* (autophagy and apoptosis genes), and *GLUT-1* (a glucose transport gene), we observed that HT1080 cells in 3D hydrogel adapted better to hypoxic conditions than those in a Petri dish, with no obvious correlation to matrix viscoelasticity, by recovering rapidly from possible autophagy/apoptotic events and alternating metabolism mechanisms. Further, we examined how HT1080 cells cultured in varying viscoelasticity and oxygen tension conditions affected endothelial sprouting and invasion. We observed that increased matrix stiffness reduced endothelial sprouting and invasion in atmospheric conditions; however, we observed increased endothelial sprouting and invasion under hypoxia at all levels of matrix stiffness with the upregulation of vascular endothelial growth factor (*VEGF*) and angiopoeitin-1 (*ANG-1*). Overall, HT1080 cells encapsulated in the AHA hydrogels under hypoxic stress recovered better from apoptosis and demonstrated greater angiogenic induction. Thus, we propose that oxygen tension more profoundly influences cell fate and the angiogenic potential of 3D cultured HT1080 fibrosarcoma cells than does matrix stiffness.

[*]Address for reprint request and other correspondence: S. Gerecht, Department of Chemical and Biomolecular Engineering, Johns Hopkins University Maryland Hall #116, Baltimore, MD 21218 Telephone: (410) 516-2846. gerecht@jhu.edu. Fax: (410) 516-5510.

Three-dimensional (3D) cell culture models recapitulate aspects of the *in vivo* extracellular matrix (ECM) microenvironment, allowing the study of tumor development and progression under pathologically relevant culture conditions [1–5]. Specifically, hydrogels are structurally and mechanically similar to the native ECM of many tissues and have been utilized as matrices to study cellular responses to a range of microenvironmental signals [6–8]. Hydrogels composed of natural matrices have inherently limited tunability for independently studying effects of several physiochemical properties on cellular responses, since changes in features such as mechanics and adhesion are coupled [9–11].

In contrast, engineered hydrogels that mimic various cues of the tumor microenvironment and ECM-cell interactions can be used to study the independent and codependent effects of specific cues in the microenvironment on cancer cell responses [5, 12]. For example, highly porous scaffolds fabricated from synthetic poly(lactide-co-glycolide) have been used to generate an *in vitro* human tumor model that exhibits microenvironmental conditions representative of tumors *in vivo* [13]. More recently, Gill et al. utilized a synthetic polymer-based scaffold composed primarily of polyethylene glycol, which offers biospecific cell adhesion and cell-mediated proteolytic degradation with independently adjustable matrix stiffness. They demonstrated that altering both matrix stiffness and the concentration of cell-adhesive ligand significantly influenced epithelial morphogenesis of a metastatic cell line (344SQ) [14]. ECM rigidity has been show to alter tumor cell proliferation and migration [25, 26] and resistance to chemotherapeutics [26]. Similarly, ECs have been found to change their behavior and morphology depending on substrate stiffness [27, 28]. Hence, engineering the mechanical stiffness of hydrogel, while decoupling it from other key properties such as cell adhesion, may elucidate how the tumor's physical environment contributes to its growth and angiogenesis.

Along with the adhesive and mechanical properties of the microenvironment, hypoxia is an important determinant of cell behavior. Hypoxia occurs when the partial pressure of $O_2$ falls below 5 %, inducing myriad cellular and systemic adaptations [15, 16]. In fact, during tumor growth, cells inevitably experience depletion of nutrients, including oxygen due to extensive growth [17]. Cellular responses to hypoxia are primarily regulated by hypoxia-inducible factors that accumulate under hypoxic conditions and activate numerous pathways that regulate a variety of cellular activities [18–22], such as promoting tumor growth and angiogenesis during embryonic development [17, 23, 24].

Hyaluronic acid (HA), a glycosaminoglycan abundantly present in the ECM, holds potential as an important component of matrices for the study of cancers and angiogenic responses, since it may facilitate cancer progression, invasion, migration, and angiogenesis [29]. Previously, we engineered a modular culture system using an acrylated HA (AHA) hydrogel to generate a functional human microvascular network [30] and to induce endothelial cell (EC) sprouting and angiogenesis [31]. This same AHA hydrogel system may be useful for studying how hypoxia and stiffness cues in the tumor microenvironment affect cancer cell fate (Figure 1A). The AHA macromers contain acrylate groups that react with thiols in a Michael-type addition reaction, such that crosslinking can occur with a dithiol and chemical modification can occur with a monothiol. Specifically, we crosslinked AHA with an enzymatically degradable peptide (with a sequence susceptible to matrix metalloproteinases

[MMPs] -1 and -2) that contained two cysteines and incorporated adhesion through a peptide (i.e., RGD) that contained one cysteine, where the cysteines provided thiol groups to react with acrylates. This system enables us to alter the hydrogel's crosslinking density by changing the amount of MMP crosslinker added while maintaining the overall backbone and adhesion site concentration (Figure 1B). With this approach, we generated three hydrogel matrices with distinctive levels of viscoelasticity: soft (78±16Pa); medium (309± 57Pa) and stiff (596± 73Pa; Figure 1C).

We first examined cancer cell encapsulation in the AHA hydrogels with defined viscoelasticity. For our studies, we chose a fibrosarcoma-derived cell line, HT1080, which tends to be highly angiogenic, mobile, and metastatic, making it a good candidate for the soft tissue viscoelasticity range [32–34]. We noticed that, after 24 hours of encapsulation, HT1080 cells in both medium and stiff hydrogels began to spread, but they started to form aggregates in the softest hydrogels (data not shown). Within 72 hours, most of the HT1080 cells encapsulated in stiff and medium hydrogels had spread, while most of those in the soft hydrogels aggregated into clumps and spread only occasionally (Figure 2A). Examining the viscoelasticity, we first noticed that after cell encapsulation, the stiffness of the hydrogels slightly altered to soft (66±13Pa); medium (361± 65Pa) and stiff (485± 63Pa) constructs; we also found that all constructs types, but not hydrogels alone, became softer along the culture period, reaching 14±10Pa; 77±49Pa; and 96±71Pa in the soft, medium, and stiff hydrogels, respectively. (Figure 2B). Indeed, due to the cell clusters, constructs made of soft gels became unstable and difficult to maintain, with many clusters falling off the AHA hydrogels. Thus, the studies were limited to the first three days of encapsulation of HT1080 cells.

We next determined the oxygen tension and gradients throughout the hydrogel matrices. Our previous studies showed that dissolved oxygen (DO) levels decrease during 2D culture of various human cell types [35] and that these decreases become even more dramatic in 3D hydrogel cultures, which require higher cell-seeding concentrations [36]. Indeed, in a 3D hydrogel culture system, the availability of DO to the cells depends on both oxygen diffusion from the air to the culture media and the oxygen consumption of the encapsulated cells. The oxygen consumption rate of cells depends on their spatial density and oxygen uptake rate, which is assumed to follow Michaelis-Menten kinetics. Therefore, we first determined the $V_{max}$ and $K_m$ parameters of HT1080 fibrosarcoma cells. We measured DO levels in culture media of HT1080 cells until they reached steady state. We plotted the oxygen consumption rate of the HT1080 cells (experimental data) and the theoretical Michaelis-Menten equation (numerical model) using the initial $V_{max}$ and $K_m$ values. We then calibrated the graphs while varying the $V_{max}$ and $K_m$ parameters to obtain the best fit to the experimental values according to the residual sum of squares (RSS) method (Figure 3A). We determined that the $V_{max}$ and $K_m$ values of HT1080 cells were $83.19 \times 10^{-18}$ mol/s and 66 μM, respectively. Mathematical modeling then projected [37, 38] equilibrium oxygen tension distributions at different boundary conditions (1, 5, and 21 %) with different cell encapsulation densities (1, 5, and $10 \times 10^6$ cells/ml; Figure 3B). We found that, during the initial culture period, DO gradients were generated throughout the thickness of the hydrogel. Specifically, cells at the center regions of the hydrogel experienced lower oxygen tensions

than either those in the experimental setup (i.e., air gas) or those at the edge of the hydrogel. In atmospheric conditions, HT1080 cells encapsulated at $10 \times 10^6$ cells/ml % experienced around 13 % $O_2$ at the center, compared to 17 % $O_2$ at the edge after 30 minutes of gel formation (Figure 3C). At 5 % $O_2$, while encapsulation densities of $5 \times 10^6$ cells/ml or $10 \times 10^6$ cells/ml led to oxygen levels below 2 % at the center of the hydrogel, at the $1 \times 10^6$ cells/ml encapsulation density, cells experienced a relatively uniform distribution of 5 % oxygen tension throughout the hydrogel (Figure 3D). At 1 % $O_2$, encapsulation of $5 \times 10^6$ cells/ml or $10 \times 10^6$ cells/ml resulted in anoxic conditions at the center of the hydrogel, while encapsulation of $1 \times 10^6$ cells/ml yielded oxygen levels below 0.4 % at the center (Figure 3E). Based on this analysis, we decided that using $1 \times 10^6$ cells/ml in a 5 % setup would allow us to study the responses of HT1080 cells to varying stiffnesses in conditions that support uniform DO levels throughout the hydrogel. This setting also mimics the initial circulating cancer cell attachment environment, which is marked by low cell density and moderate hypoxia [39].

Many cancer cells are shed into circulation every day. However, very few of them survive and become metastatic [40]. Rate-limiting steps at the metastatic site pose challenges to circulating cancer cells in their interaction with their microenvironment [39], where they can meet several fates (death, dormancy, or survival) modulated by the microenvironment. For example, some cancer cells stay quiescent or dormant and only later become triggered into a proliferative state for angiogenic purposes [41]. Other tumor cells enter the apoptotic/necrotic pathway. To determine the effect of hypoxia on HT1080 cell fates at different matrix stiffnesses, cells were cultured in serum-free media to synchronize their $G_0$ stages before encapsulation. After encapsulation, AHA-HT1080 constructs were cultured under atmospheric and hypoxic condition for three days. We could not observe morphological differences between 3D HT1080 cells cultured under atmospheric and hypoxic conditions (data not shown). To examine cell growth, we stained the cells with Ki67 proliferation marker. While we detected overall reduced proliferation in the 3D AHA hydrogel compared to Petri dish control, we could not detect a significant difference in proliferating cells between hypoxic and atmospheric conditions in any of the cultures examined (Figure 4A). Daily cell cycle analysis further revealed no significant differences in population percentage at the S phase or $G_2$ phase (Supplementary Figure 1), suggesting that, over the 72 hours, HT1080 cells divide at a similar rate in all conditions examined. We noticed that, 24 hours following encapsulation, HT1080 cells experienced apoptosis (indicated by the sub-$G_1$ population) and that, under hypoxia, they recover better, resulting in significantly lower percentages of apoptotic cells after 48 hours (Figure 4B–C). Matrix stiffness seemed to affect recovery from cell apoptosis minimally. After 24 hours under hypoxic conditions, HT1080 cells encapsulated in matrix with medium stiffness experienced high levels of apoptotic events compared to cell encapsulated in soft or stiff matrices. We therefore examined the upregulation of the autophagy gene of the BCL-2 family, BCL-2/adenovirus E1B 19 kDa-interacting protein 3 (*BNIP3*) [42], and the proapoptotic gene Bnip3-like protein X (*BNIP3L*), also of the BCL-2 family, in HT1080 cells encapsulated in medium AHA hydrogels. While we could not detect differences in the expression of *BNIP3L* (data not shown), upregulation in the expression of *BNIP3* was detected 24 hours following encapsulation and was downregulated after 48 hours of culture (Figure 4Di). The same

expression pattern could also be detected for glucose transport (*GLUT-1*) in hypoxic HT1080 cells (Figure 4 Dii). When HT1080 cells were cultured in a Petri dish, hypoxia upregulated the expression of GLUT-1 and BNIP3 after 24 hours, which further increased after 48 hours, suggesting a rapid response and adaptation to the oxygen conditions within the 3D AHA culture microenvironment (Figure 4D). These results suggest the adaptation of HT1080 cells under hypoxic conditions, rapidly recovering from possible autophagy events and alternating metabolism mechanisms. This also suggests that HT1080 cells, when cultured in AHA hydrogel under atmospheric conditions, experience apoptosis induced by a different mechanism than those examined here. Overall, these results suggest that hypoxia and, to a lesser extent, hydrogel stiffness affected cell fate throughout the three-day study.

Finally, we sought to examine the ability of 3D encapsulated HT1080 cells to induce endothelial sprouting under hypoxia at different matrix stiffnesses. Davis and colleagues developed an *in vitro* angiogenesis assay using collagen gels [43, 44]. They showed that, in response to sphingosine-1-phosphate (S1P) and stromal cell-derived factor-1 (SDF-1α), a confluent monolayer of ECs invaded and sprouted into the collagen gels underneath in a way that mimicked the appearance of tip cells from preexisting blood vessels [44]. We previously adapted this approach and showed that AHA hydrogels could serve as an *in vitro* angiogenesis assay and, as such, provide opportunities to elucidate the role of matrix remodeling during angiogenesis in synthetic biomaterials [45]. In this earlier study, we found that endothelial colony-forming cells (ECFCs) cultured on top of the medium AHA matrix loaded with SDF1-α and S1P sprouted and invaded the hydrogel in atmospheric conditions. These results suggest that, with the necessary adhesion and degradation properties, low viscoelasticity, and cytokine stimuli, ECs can sprout and invade such AHA hydrogels. In the current study, we modified this approach and encapsulated HT1080 cells with SDF-1α and S1P for 24 hours in atmospheric or hypoxic conditions, following which we seeded a monolayer of ECFCs and analyzed their sprouting and invasion into the AHA hydrogels after a further 24 hours in atmospheric conditions (Figure 5A). AHA hydrogel encapsulating only SDF-1α and S1P served as controls. It should be noted that HT1080 cells encapsulated without the addition of SDF-1α and S1P induced little to no EC sprouting and invasion. We observed similar EC sprouting and invasion into soft-matrix-encapsulated HT1080 cells in atmospheric and hypoxic conditions. While EC sprouting was observed in HT1080 constructs with medium viscoelasticity cultured in atmospheric conditions, a significant increase in sprouting length was observed in hypoxic conditions. Finally, HT1080 cells encapsulated in stiff hydrogels underwent EC sprouting and invasion in hypoxic but not in atmospheric conditions (Figure 5B–C). Overall, we found that, in atmospheric conditions, softer matrices promoted EC sprouting and invasion, corresponding to similar cellular events during vasculogenesis [30, 31, 45–49]. In hypoxia, while the lowest angiogenic response occurred in the stiff matrix, soft and medium hydrogels had similarly higher responses. Gene expression analysis of HT1080 cells after 24 hours in 3D culture revealed the upregulated expression of MMP-1 in hypoxic HT1080 cells within stiff hydrogels, suggesting that the cells may alter the viscoelastic properties of these hydrogels under hypoxic conditions, enabling EC sprouting and invasion (Figure 6A). Indeed, when we examined HT1080 construct viscoelasticity, we found that after 24 hours in hypoxic conditions, all constructs became significantly softer; stiff constructs reached 127±98Pa;

medium constructs reached 61±60Pa; and soft constructs reached 4±4Pa (Figure 6B). Gene expression analysis of the angiogenic factors vascular endothelial growth factor (*VEGF*) and angiopoeitin-1 (*ANG-1*) showed that hypoxia upregulated secretion of these angiogenic factors by the HT1080 cells more than atmospheric conditions (Figure 6C–D) also, we observed a greater upregulation of these factors in cells cultured in a 3D than in a 2D environment. These factors most likely contribute to the angiogenic state of the ECFCs.

Overall, our results imply that oxygen tension influences 3D cultured HT1080 cells more profoundly than matrix stiffness. Encapsulated in the AHA hydrogels under hypoxic stress, HT1080 cells recovered from apoptosis better and demonstrated greater angiogenic induction. While it seems surprising that matrix stiffness plays a minimal role in determining cell fate and triggering the angiogenic capability of HT1080 cells, it is possible that conducting experiments over longer time periods or examining a wider viscoelasticity range would activate signaling pathways that are dependent on stiffness mechanism in 3D constructs. In the study of EC sprouting, it is worth noting that, without the addition SDF-1α and S1P, we observed little or no sprouting, suggesting that other cell types in the tumor microenvironment secrete these two (or similar) growth factors. Candidates include stromal cells or leukocytes, which are recruited toward malignant cell sites and produce S1P or SDF-1 [39, 50].

## Conclusions

Utilizing AHA hydrogels, we generated a well-defined 3D culture system to study the effects of matrix viscoelasticity and oxygen tension on cancer cell behavior. We found that encapsulation of 5 to 10 × $10^6$ cells/ml generated DO gradients throughout the hydrogel matrix in atmospheric (21 %), hypoxic (5 %), and severely hypoxic (1 %) conditions. Encapsulation of low cell concentrations (1 × $10^6$ cells/ml) maintained a uniform DO distribution under atmospheric and hypoxic conditions. We demonstrated that, using our 3D AHA hydrogel culture system, encapsulated HT1080 cells recovered more rapidly from apoptosis under hypoxic conditions than under atmospheric conditions without obvious correlation to the matrix's stiffness. We found that angiogenic induction correlated highly to decreases in matrix stiffness under atmospheric conditions, while hypoxia upregulated angiogenic responses in the stiffer hydrogels. Overall, we suggest that hypoxic pathways activation of HT1080 cells encapsulated in the 3D AHA hydrogel enables better cell survival and supports EC sprouting. Other potential uses for this system including comparing the responses of different cancer cell lines at different stages of tumorigenesis, supporting the basic study of tumor biology, and selectively impeding cancerous processes.

## MATERIALS AND METHODS

### Cell culture

HT1080 cells (ATCC, Manassas, Virginia) were cultured according to the manufacturer's instructions in Dulbecco's Modified Eagle's medium (DMEM, GIBCO) supplemented with 10 % fetal bovine serum (FBS GIBCO). For cell encapsulation and cell cycle studies, HT1080 cells were synchronized under serum-free media for three days with daily media change. Human umbilical cord blood ECFCs were provided by Dr. Merv C. Yoder, Indiana

University School of Medicine, and expanded and used for experiments between passages 6 and 9, as previously described [30, 31]. ECFCs were cultured in flasks precoated with type I collagen (Roche Diagnostics, Basel, Switzerland), in endothelial growth medium (EGM, PromoCell, Heidelberg, Germany) supplemented with 1 ng/ml $VEGF_{165}$ (Pierce, Rockford, IL). All cell cultures were incubated in a humidified incubator at 37 °C in an atmosphere containing 5 % $CO_2$. Both HT1080 cells and ECFCs were passaged every four to five days with 0.05 % trypsin (Invitrogen, Carlsbad, CA), and media were changed every other day.

## Macromer synthesis

AHA macromer synthesis was performed as reported previously [51]. Briefly, we synthesized AHA in two steps: (1) the tetrabutyl-ammonium salt of HA (HA-TBA) was formed by reacting sodium hyaluronate (90 kDa; LifeCore Biomedical, Chaska, MN) with the ion exchange resin Dowex-100 (Sigma) and neutralizing with 0.2 M TBA-OF (Sigma); (2) acrylic acid (3 [eq]) and HA-TBA (1 eq) were coupled in the presence of dimethylaminopyridine (DMAP; 0.15 eq) and di-tert-butyl dicarbonate (3 eq) in DMSO, followed by dialysis and lyophilization. We used $^1$H NMR spectra to confirm the modification of the AHA. The cell-adhesive peptide GCGYGRGDSPG (RGDS, molecular weight [MW]: 1025.1 Da) and MMP-sensitive peptide crosslinker GCRDGPQGWGQDRCG (MMP, MW: 1754 Da) were purchased (Genscript; greater than 95 % purity, per manufacturer's HPLC analysis).

## Hydrogel formation and cell encapsulation

For hydrogel formation, AHA macromer was dissolved in triethanolamine-buffered saline (TEOA buffer: 0.2 M TEOA) at 3 % w/w. The cell adhesive peptides (RGDS, GenScript) were dissolved in TEOA buffer and added to the AHA solution to reach a final peptide concentration of 3.8 mM and allowed to react for one hour with gentle shaking. For crosslinking, MMP crosslinker (MMP, GenScript) dissolved in TEOA buffer was added to reach a final concentration of 2.57 mM (soft) 5.15 mM (medium), or 10.3mM (stiff). Hydrogels were allowed to swell for three hours prior to mechanical testing. The elastic modulus (G') was measured using a constant strain rheometer with steel cone plate geometry (25 mm in diameter; RFS3; TA Instruments). The strain was maintained at 20 % during the time sweeps by adjusting the stress amplitude at a frequency of 10 Hz. Three samples were tested for each gel. The tests occurred in a humidified chamber at a constant temperature (25 °C) at 30-second intervals. We then calculated Young's elastic modulus using $E = 2G'(1 + v)$. Assuming the hydrogel is incompressible, the Poisson ratios (v) approach 0.5, and the relationship becomes $E=3G'$. The same approach was used to measure the constructs along the culture period.

Preconditioned HT1080 cells were encapsulated in HA hydrogels with densities of 1, 5, and $10 \times 10^6$ cells/ml by suspending the cells in HA-RGD solution, as above, prior to addition of the MMP crosslinker. We pipetted 50 μl of the final mixture into sterile molds and allowed it to react for ten minutes at room temperature in a laminar flow hood. The constructs were then cultured in HT1080 growth media in the conditions described throughout this paper.

### Oxygen tension modeling and hypoxia experiments

Oxygen tension profiles were modeled within the gels following a previously established method for collagen gels [36]. Briefly, to estimate DO gradients in 3D AHA gels, we first determined the $V_{max}$ and $K_m$ parameters of HT1080 cells in 3D AHA 3 % w/w gel. We attached oxygen sensor patches (Presens, Regensburg, Germany) to the bottoms of the 96-well plates. Cells were then seeded at 2 million cells/ml with 50 μl of media in the well. Next, we sealed the well completely, to provide a closed system for oxygen measurement, and allowed them to reach anoxia. Using DO level data measured continuously, we estimated $V_{max}$ and $K_m$ using the RSS method to find the best fit between analytical and numerical data. We then used the Michaelis-Menten parameters determined for the given conditions to estimate the DO gradients throughout the gel depth, using the commercial software package Comsol Multiphysics (Comsol, Los Angeles, CA). AHA constructs were modeled within culture media, allowing oxygen permeability in all directions. Hypoxia (5 % $O_2$) experiments were conducted as described previously [52]. Briefly, cells were cultured in a hermetically sealed, humidified modular incubator chamber (Billups-Rothenberg, Del Mar, CA, USA), which was flushed with an appropriate gas mixture (a 5 % $O_2$/5 % $CO_2$/$N_2$ balance) three times every 30 minutes at the beginning of each experiment. Placing a plastic Petri dish containing 10 ml of sterile water on the chamber bottom maintained humidity during experiments.

### Flow cytometry and cell cycle analysis

Flow cytometry was performed for cell cycle analysis and proliferation. Briefly, encapsulated HT1080 cells were exposed to hypoxia at 5 % $O_2$ tension for up to three days. Gels were harvested at desired time points and digested with hyaluronidase (Sigma) for ten minutes and then 0.25 % trypsin for five minutes to dissociate the cell from the hydrogel. The samples were then centrifuged to separate gels and cells. Next, we fixed the cell pellets in ice-cold 70 % ethanol overnight at 4 °C. Triton X-100 (0.1 %) and RNase A (100 μg/ml; Qiagen, Valencia, CA) were added to obtain a final concentration of $10^6$ cells/ml, and cells were incubated in the solution for two hours at 37 °C before being stained with 50 μg/ml propidium iodide (Sigma Aldrich, St. Louis, MO) for 15 minutes at 37 °C. For proliferation, constructs were fixed with ethanol, harvested using hyaluronidase, stained with anti-human Ki67 (Life Technology) for 30 minutes, and washed with PBS. To avoid clumping, we strained the cells through a 40 μm cell strainer. Cell cycles were analyzed with the BD FACSCalibur flow cytometer (Becton Dickinson, NJ), reading the signals detected by FL2. Data were analyzed using FlowJo software, version 7.5, to determine the frequencies of each cell cycle phase.

### Quantitative RT-PCR

Two-step RT-PCR was performed for *VEGF*, *ANG-1*, *MMP-1*, *GLUT-1*, *BNIP3*, *BNIP3L*, *18S*, *GAPDH*, and *beta-actin*, and samples were examined in triplicate, analyzed, and graphed. Briefly, RNA was extracted using TRIzol (GIBCO) according to the manufacturer's instructions. Total RNA was quantified by nanodrop spectrophotometer. Gene expression assays were performed on an Applied Biosystems StepOne Real-Time PCR system according to the manufacturer's instructions. The relative expression of genes was

normalized to the indigenous control genes. The comparative CT method was used to calculate amplification differences on targeted genes. The values for experiments (n=3) were averaged and graphed.

### 2D sprouting assay

2D sprouting assays to assess the sprouting potential were based on previously established methods using collagen or fibrin gels [31, 53]. AHA hydrogels were prepared as described above, with or without the encapsulation of HT1080 cells or with the addition of sphingosine-1-phosphate (S1P, Avanti Polar Lipids) and stromal cell-derived factor-1 (SDF-1, R&D Systems) at a concentration of 125 μM. ECFCs were seeded on top of the AHA hydrogels and cultured for an additional 24 hours to allow invasion into the gels. Samples were then fixed and processed for fluorescence staining and further image analysis (see below).

### Fluorescence staining

Following sprouting assay, ECFC-HT1080 constructs were fixed using formalin for 30 minutes and washed with PBS. For staining, the constructs were permeabilized with a solution of 0.1 % Triton-X for 15 minutes, washed with PBS, stained with fluorescein-conjugated UEA-I lectin for two hours, rinsed, and then stained with DAPI for 15 minutes. The labeled samples were examined using a side view perpendicular to the sprouting direction by either fluorescence microscopy (Olympus BX60; Olympus, Center Valley, PA) or confocal microscopy (LSM 510 Meta; Carl Zeiss). To analyze the sprouting length of ECFCs, measurement tools in Image J (NIH) were used and normalized to the medium gel without encapsulated cancer cells under atmospheric conditions while keeping all other formulations the same; this served as a positive control and reference point across different sets of experiments.

### Statistical analysis

All experiments and assays were performed on at least triplicate samples with triplicate readings. Graphs were plotted with standard deviation (SD). Significance levels were determined using unpaired two-tailed t-tests or two-way ANOVA where appropriate (GraphPad Prism 4.02). Significance levels were determined using post-tests with *P<.05, **P<.01 and ***P<.001.

## Supplementary Material

Refer to Web version on PubMed Central for supplementary material.

## Acknowledgments

We thank Sravanti Kusuma for reviewing the manuscript. This research was partially funded by a pilot project from the National Institute of Health grant U54CA143868 (to SG and JAB) and National Science Foundation grant 1054415 (to SG).

## References


1. Gurski LA, Jha AK, Zhang C, Jia XQ, Farach-Carson MC. Hyaluronic acid-based hydrogels as 3D matrices for in vitro evaluation of chemotherapeutic drugs using poorly adherent prostate cancer cells (vol 30, pg 6076, 2009). Biomaterials. 2010; 31:4248.
2. Szot CS, Buchanan CF, Freeman JW, Rylander MN. 3D in vitro bioengineered tumors based on collagen I hydrogels. Biomaterials. 2011; 32:7905–7912. [PubMed: 21782234]
3. Yamada KM, Cukierman E. Modeling tissue morphogenesis and cancer in 3D. Cell. 2007; 130:601–610. [PubMed: 17719539]
4. Nyga A, Cheema U, Loizidou M. 3D tumour models: novel in vitro approaches to cancer studies. J Cell Commun Signal. 2011; 5:239–248. [PubMed: 21499821]
5. Hielscher AC, Gerecht S. Engineering approaches for investigating tumor angiogenesis: exploiting the role of the extracellular matrix. Cancer Res. 2012; 72:6089–6096. [PubMed: 23172313]
6. Discher DE, Janmey P, Wang Y-l. Tissue Cells Feel and Respond to the Stiffness of Their Substrate. Science. 2005; 310:1139–1143. [PubMed: 16293750]
7. Engler AJ, Sen S, Sweeney HL, Discher DE. Matrix elasticity directs stem cell lineage specification. Cell. 2006; 126:677–689. [PubMed: 16923388]
8. Ghosh K, Pan Z, Guan E, Ge S, Liu Y, Nakamura T, et al. Cell adaptation to a physiologically relevant ECM mimic with different viscoelastic properties. Biomaterials. 2007; 28:671–679. [PubMed: 17049594]
9. Reiser K, McCormick RJ, Rucker RB. Enzymatic and nonenzymatic cross-linking of collagen and elastin. FASEB J. 1992; 6:2439–2449. [PubMed: 1348714]
10. Robins SP. Biochemistry and functional significance of collagen cross-linking. Biochem Soc Trans. 2007; 35:849–852. [PubMed: 17956230]
11. Cross VL, Zheng Y, Choi NW, Verbridge SS, Sutermaster BA, Bonassar LJ, et al. Dense type I collagen matrices that support cellular remodeling and microfabrication for studies of tumor angiogenesis and vasculogenesis in vitro. Biomaterials. 2010; 31:8596–8607. [PubMed: 20727585]
12. Verbridge SS, Chandler EM, Fischbach C. Tissue-engineered three-dimensional tumor models to study tumor angiogenesis. Tissue Eng Part A. 2010; 16:2147–2152. [PubMed: 20214471]
13. Fischbach C, Chen R, Matsumoto T, Schmelzle T, Brugge JS, Polverini PJ, et al. Engineering tumors with 3D scaffolds. Nature methods. 2007; 4:855–860. [PubMed: 17767164]
14. Gill BJ, Gibbons DL, Roudsari LC, Saik JE, Rizvi ZH, Roybal JD, et al. A synthetic matrix with independently tunable biochemistry and mechanical properties to study epithelial morphogenesis and EMT in a lung adenocarcinoma model. Cancer Res. 2012; 72:6013–6023. [PubMed: 22952217]
15. Gordan JD, Simon MC. Hypoxia-inducible factors: central regulators of the tumor phenotype. Current opinion in genetics & development. 2007; 17:71–77. [PubMed: 17208433]
16. Wang GL, Semenza GL. Purification and characterization of hypoxia-inducible factor 1. The Journal of biological chemistry. 1995; 270:1230–1237. [PubMed: 7836384]
17. Heddleston JM, Li Z, Lathia JD, Bao S, Hjelmeland AB, Rich JN. Hypoxia inducible factors in cancer stem cells. British journal of cancer. 2010; 102:789–795. [PubMed: 20104230]
18. Manalo DJ, Rowan A, Lavoie T, Natarajan L, Kelly BD, Ye SQ, et al. Transcriptional regulation of vascular endothelial cell responses to hypoxia by HIF-1. Blood. 2005; 105:659–669. [PubMed: 15374877]
19. Ramirez-Bergeron DL, Simon MC. Hypoxia-inducible factor and the development of stem cells of the cardiovascular system. Stem Cells. 2001; 19:279–286. [PubMed: 11463947]
20. Maltepe E, Simon MC. Oxygen, genes, and development: an analysis of the role of hypoxic gene regulation during murine vascular development. J Mol Med. 1998; 76:391–401. [PubMed: 9625296]
21. Fong GH. Regulation of angiogenesis by oxygen sensing mechanisms. J Mol Med. 2009; 87:549–560. [PubMed: 19288062]

22. Yamakawa M, Liu LX, Date T, Belanger AJ, Vincent KA, Akita GY, et al. Hypoxia-inducible factor-1 mediates activation of cultured vascular endothelial cells by inducing multiple angiogenic factors. Circ Res. 2003; 93:664–673. [PubMed: 12958144]
23. Simon MC, Keith B. The role of oxygen availability in embryonic development and stem cell function. Nature reviews Molecular cell biology. 2008; 9:285–296.
24. Jopling C, Sune G, Faucherre A, Fabregat C, Izpisua Belmonte JC. Hypoxia induces myocardial regeneration in zebrafish. Circulation. 2012; 126:3017–3027. [PubMed: 23151342]
25. Pathak A, Kumar S. Independent regulation of tumor cell migration by matrix stiffness and confinement. Proc Natl Acad Sci U S A. 2012; 109:10334–10339. [PubMed: 22689955]
26. Schrader J, Gordon-Walker TT, Aucott RL, van Deemter M, Quaas A, Walsh S, et al. Matrix stiffness modulates proliferation, chemotherapeutic response, and dormancy in hepatocellular carcinoma cells. Hepatology. 2011; 53:1192–1205. [PubMed: 21442631]
27. Hanjaya-Putra D, Yee J, Ceci D, Truitt R, Yee D, Gerecht S. Vascular endothelial growth factor and substrate mechanics regulate in vitro tubulogenesis of endothelial progenitor cells. J Cell Mol Med. 2010; 14:2436–2447. [PubMed: 19968735]
28. Sieminski AL, Hebbel RP, Gooch KJ. The relative magnitudes of endothelial force generation and matrix stiffness modulate capillary morphogenesis in vitro. Exp Cell Res. 2004; 297:574–584. [PubMed: 15212957]
29. Dickinson LE, Ho CC, Wang GM, Stebe KJ, Gerecht S. Functional surfaces for highresolution analysis of cancer cell interactions on exogenous hyaluronic acid. Biomaterials. 2010; 31:5472–5478. [PubMed: 20398926]
30. Hanjaya-Putra D, Bose V, Shen YI, Yee J, Khetan S, Fox-Talbot K, et al. Controlled activation of morphogenesis to generate a functional human microvasculature in a synthetic matrix. Blood. 2011; 118:804–815. [PubMed: 21527523]
31. Hanjaya-Putra D, Wong KT, Hirotsu K, Khetan S, Burdick JA, Gerecht S. Spatial control of cell-mediated degradation to regulate vasculogenesis and angiogenesis in hyaluronan hydrogels. Biomaterials. 2012; 33:6123–6131. [PubMed: 22672833]
32. Bancroft LW, Peterson JJ, Kransdorf MJ, Nomikos GC, Murphey MD. Soft tissue tumors of the lower extremities. Radiol Clin North Am. 2002; 40:991–1011. [PubMed: 12462465]
33. Al-Mehdi AB, Tozawa K, Fisher AB, Shientag L, Lee A, Muschel RJ. Intravascular origin of metastasis from the proliferation of endothelium-attached tumor cells: a new model for metastasis. Nat Med. 2000; 6:100–102. [PubMed: 10613833]
34. Krouskop TA, Wheeler TM, Kallel F, Garra BS, Hall T. Elastic moduli of breast and prostate tissues under compression. Ultrason Imaging. 1998; 20:260–274. [PubMed: 10197347]
35. Abaci HE, Truitt R, Luong E, Drazer G, Gerecht S. Adaptation to oxygen deprivation in cultures of human pluripotent stem cells, endothelial progenitor cells, and umbilical vein endothelial cells. Am J Physiol Cell Physiol. 2010; 298:C1527–C1537. [PubMed: 20181925]
36. Abaci HE, Truitt R, Tan S, Gerecht S. Unforeseen decreases in dissolved oxygen levels affect tube formation kinetics in collagen gels. American journal of physiology Cell physiology. 2011; 301:C431–C440. [PubMed: 21543738]
37. Abaci HE, Truitt R, Luong E, Drazer G, Gerecht S. Adaptation to oxygen deprivation in cultures of human pluripotent stem cells, endothelial progenitor cells, and umbilical vein endothelial cells. American journal of physiology Cell physiology. 298:C1527–C1537. [PubMed: 20181925]
38. Abaci HE, Truitt R, Tan S, Gerecht S. Unforeseen decreases in dissolved oxygen levels affect tube formation kinetics in collagen gels. American journal of physiology Cell physiology. 301:C431–C440. [PubMed: 21543738]
39. Joyce JA, Pollard JW. Microenvironmental regulation of metastasis. Nat Rev Cancer. 2009; 9:239–252. [PubMed: 19279573]
40. Chambers AF, Groom AC, MacDonald IC. Dissemination and growth of cancer cells in metastatic sites. Nat Rev Cancer. 2002; 2:563–572. [PubMed: 12154349]
41. Holmgren L, O'Reilly MS, Folkman J. Dormancy of micrometastases: balanced proliferation and apoptosis in the presence of angiogenesis suppression. Nat Med. 1995; 1:149–153. [PubMed: 7585012]

42. Zhang H, Bosch-Marce M, Shimoda LA, Tan YS, Baek JH, Wesley JB, et al. Mitochondrial autophagy is an HIF-1-dependent adaptive metabolic response to hypoxia. The Journal of biological chemistry. 2008; 283:10892–10903. [PubMed: 18281291]
43. Davis GE, Kon W, Stratman AN. Mechanisms controlling human endothelial lumen formation and tube assembly in three-dimensional extracellular matrices. Birth Defects Research Part C - Embryo Today: Reviews. 2007; 81:270–285.
44. Bayless KJ, Kwak H-I, Su S-C. Investigating endothelial invasion and sprouting behavior in three-dimensional collagen matrices. Nat Protocols. 2009; 4:1888–1898.
45. Hanjaya-Putra D, Wong K, Hirotsu K, Khetan S, Burdick JA, Gerecht S. Spatial control of cell-mediated degradation to regulate vasculogenesis and angiogenesis in synthetic hydrogels. 2012; 33(26):6123–6131.
46. Yee D, Hanjaya-Putra D, Bose V, Luong E, Gerecht S. Hyaluronic Acid hydrogels support cord-like structures from endothelial colony-forming cells. Tissue Eng Part A. 2011; 17:1351–1361. [PubMed: 21247340]
47. Hanjaya-Putra D, Yee J, Ceci D, Truitt R, Yee D, Gerecht S. Vascular endothelial growth factor and substrate mechanics regulate in vitro tubulogenesis of endothelial progenitor cells. J Cell Mol Med. 2009
48. Hanjaya-Putra D, Yee J, Ceci D, Truitt R, Yee D, Gerecht S. Vascular endothelial growth factor and substrate mechanics regulate in vitro tubulogenesis of endothelial progenitor cells. J Cell Mol Med. 2010; 14:2436–2447. [PubMed: 19968735]
49. Bayless KJ, Salazar R, Davis GE. RGD-dependent vacuolation and lumen formation observed during endothelial cell morphogenesis in three-dimensional fibrin matrices involves the alpha(v)beta(3) and alpha(5)beta(1) integrins. Am J Pathol. 2000; 156:1673–1683. [PubMed: 10793078]
50. Nagahashi M, Ramachandran S, Kim EY, Allegood JC, Rashid OM, Yamada A, et al. Sphingosine-1-phosphate produced by sphingosine kinase 1 promotes breast cancer progression by stimulating angiogenesis and lymphangiogenesis. Cancer Res. 2012; 72:726–735. [PubMed: 22298596]
51. Khetan S, Katz JS, Burdick JA. Sequential crosslinking to control cellular spreading in 3-dimensional hydrogels. Soft Matter. 2009; 5:1601–1606.
52. Abaci HE, Truitt R, Tan S, Gerecht S. Unforeseen decreases in dissolved oxygen levels affect tube formation kinetics in collagen gels. Am J Physiol-Cell Ph. 2011; 301:C431–C440.
53. Bayless KJ, Kwak HI, Su SC. Investigating endothelial invasion and sprouting behavior in three-dimensional collagen matrices. Nat Protoc. 2009; 4:1888–1898. [PubMed: 20010936]

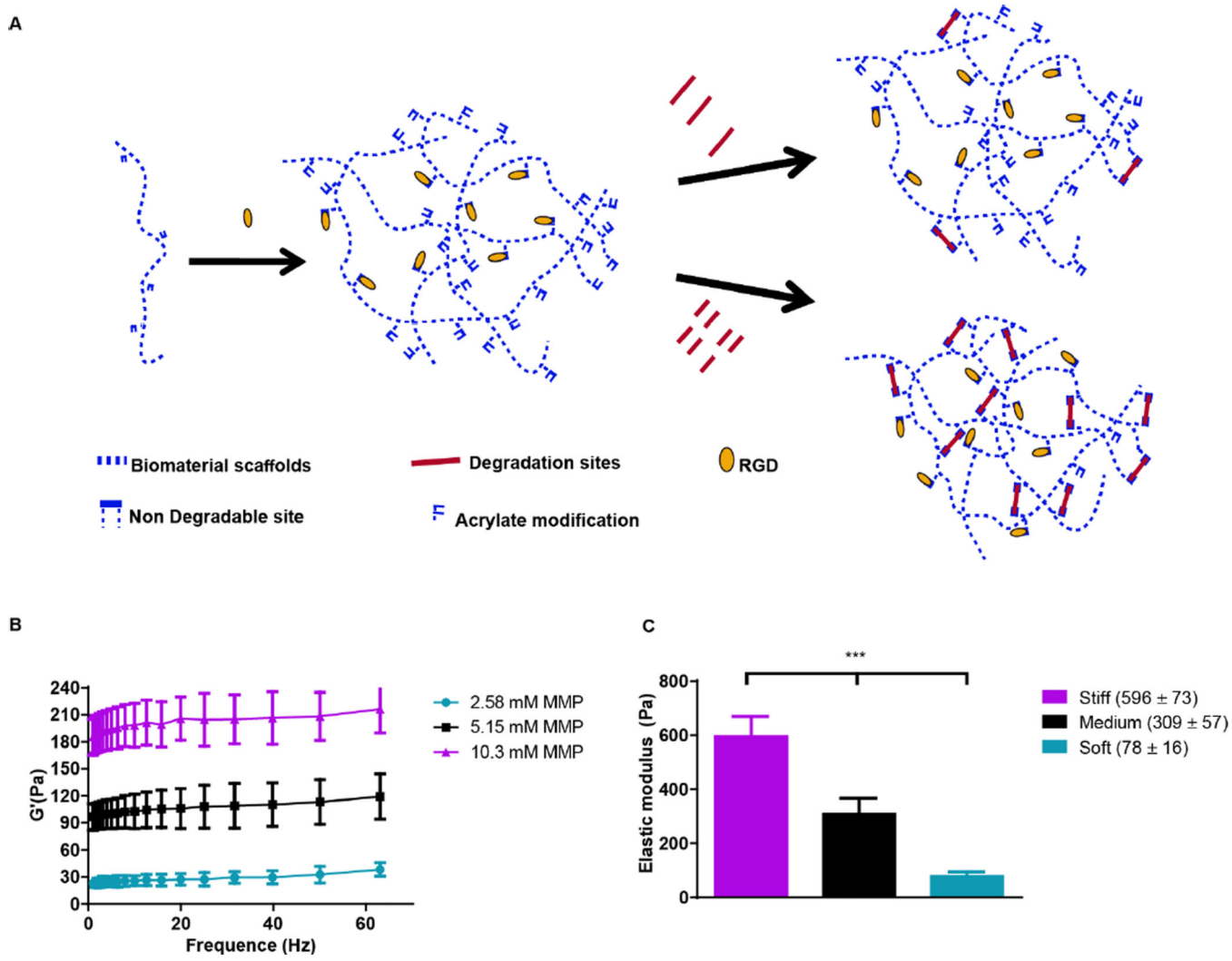


**Figure 1. Acrylated HA hydrogels**

(**A**) Schematic representation of AHA hydrogels, which are formed by reacting AHA macromers with RGD-containing peptides and MMP-sensitive crosslinkers, where the crosslinker concentration controls viscoelasticity. (**B**) Rheology frequency sweeps of AHA hydrogel with varying MMP crosslinker concentrations, showing that the modulus depends on crosslinker concentration. (**C**) Elastic modulus following polymerization and swelling: soft (78±16 Pa); medium (309± 57 Pa), and stiff (596± 73 Pa).

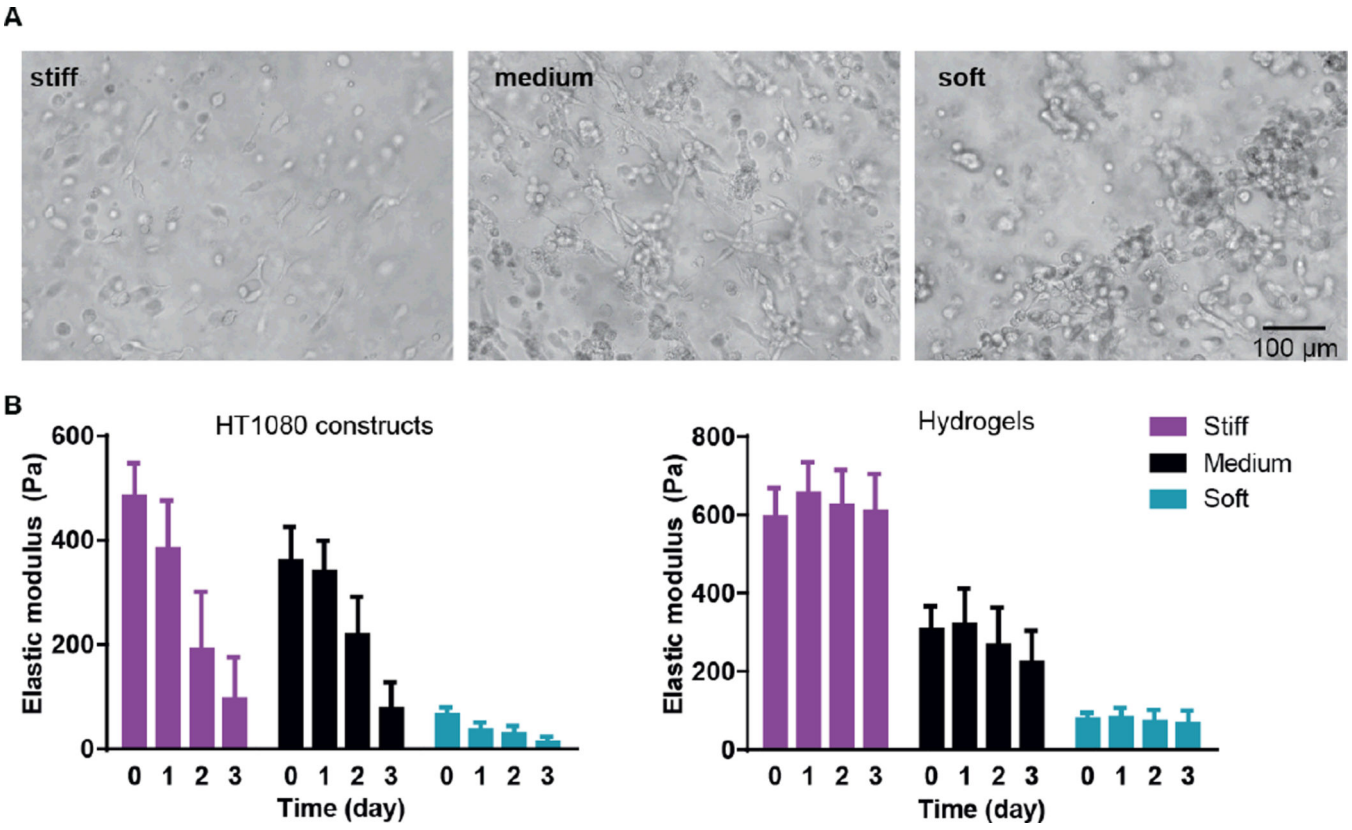


**Figure 2. HT1080 cells encapsulated in AHA hydrogels with defined stiffnesses**

(**A**) Light microscopy images of three-day culture of HT1080 cells in stiff, medium, and soft AHA hydrogels. (**B**) Viscoelasticity measurements of the different HT1080 construct types (*left*) or hydrogels alone (*right*) along the three-day culture period.

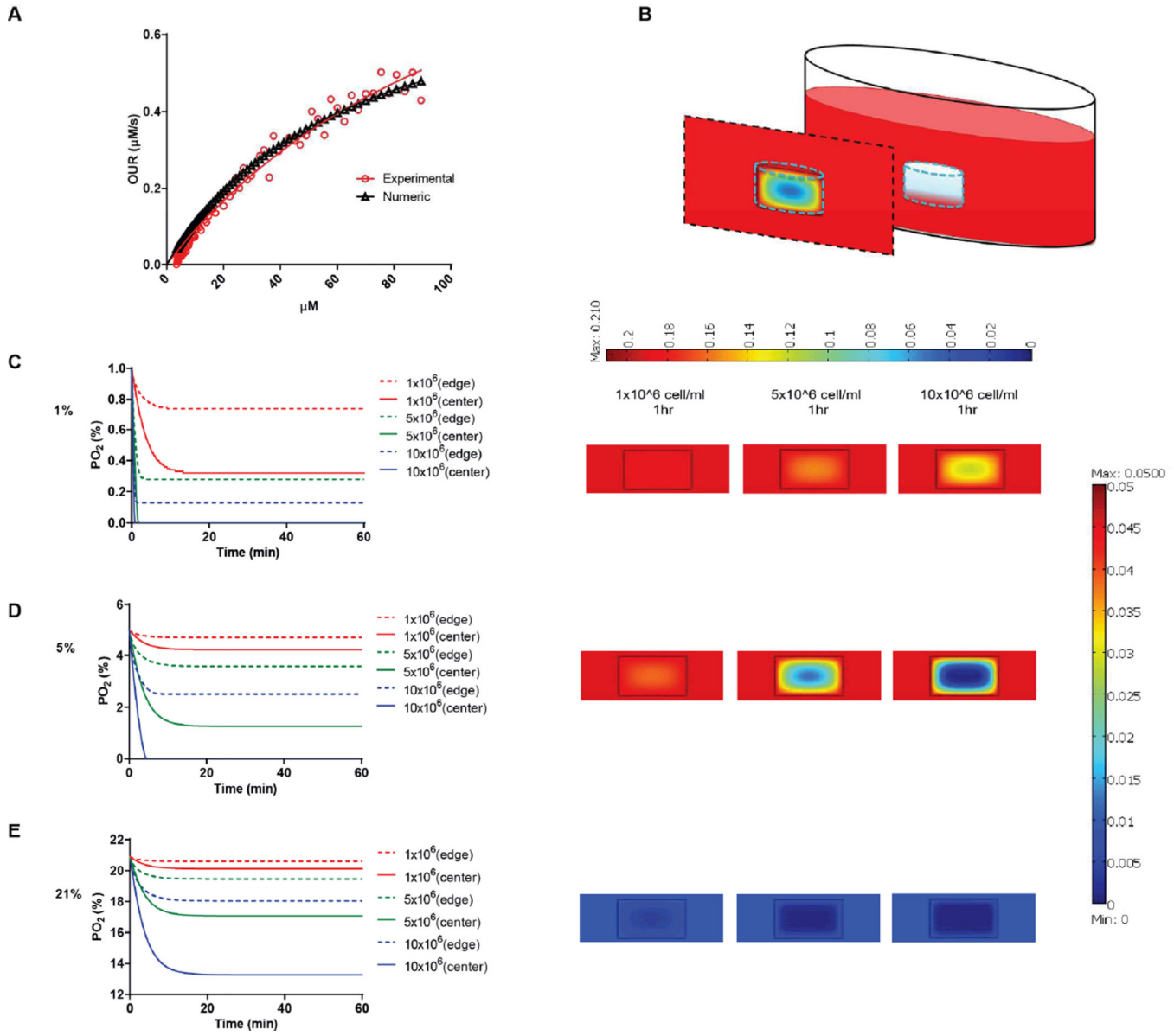


**Figure 3. Predicting DO levels in AHA hydrogels**

(**A**) Oxygen consumption rate of HT1080 cells following Michaelis-Menten kinetics. Plots were calibrated according to the residual sum of squares method to find the best fit between theoretical and experimental values. $V_{max}$ and $K_m$ values of HT1080 cells were 83.19 × $10^{-18}$ mol/s and 66 μM, respectively. (**B**) Schematic of the 3D HT1080-AHA construct in culture comprises three individual layers: (i) AHA gel containing HT1080 cells (middle layer), (ii) growth medium (surrounding layer), and (iii) air (top layer). Model prediction of DO levels within the hydrogels at (**C**) 21 %, (**D**) 5 %, and (**E**) 1 % $O_2$, with HT1080 cells encapsulated at concentrations ranging from 1 to 10 × $10^6$ cells/ml during the first hours (*left panel*: lines show DO levels at the center of the hydrogel; broken lines, the DO levels at the edge of the hydrogel), and DO gradient profile throughout the hydrogels' depth after an hour (*right panel*).

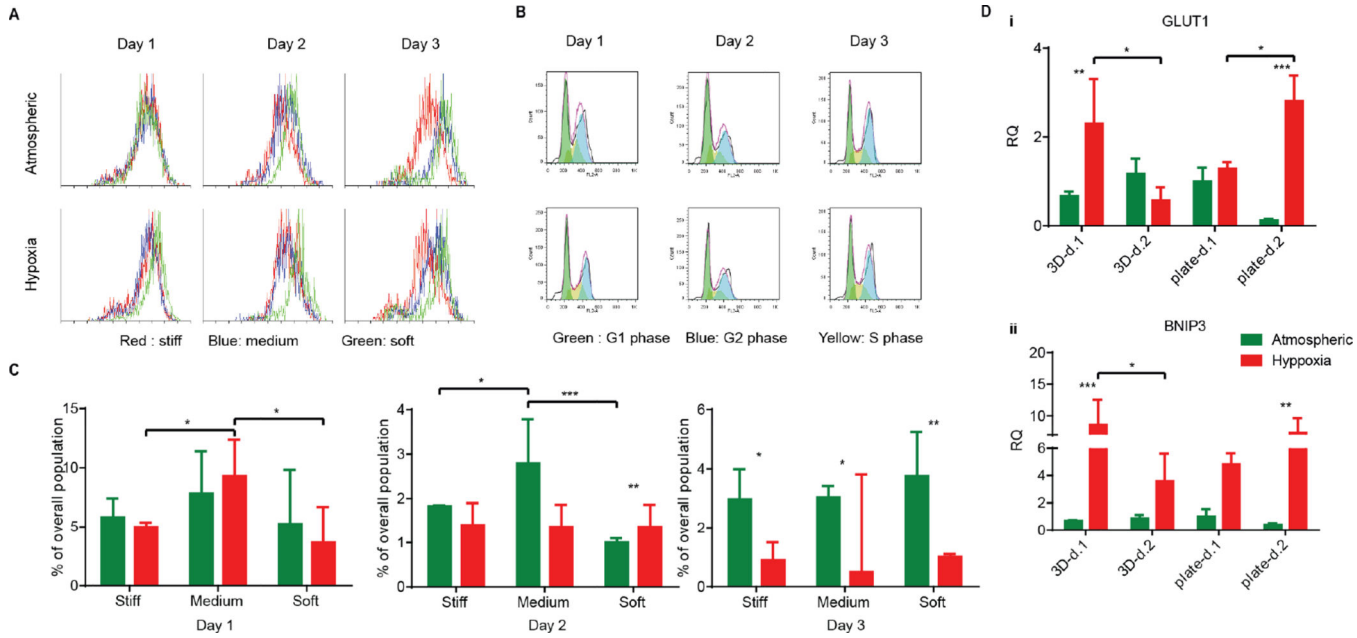


**Figure 4. HT1080 cell fate in AHA hydrogels with varying stiffnesses in atmospheric and hypoxic conditions**

(**A**) Proliferation of HT1080 cells encapsulated in stiff hydrogels over the three-day experiment in atmospheric and hypoxic conditions. (**B**) Representative cell cycle flow analysis of HT1080 cells encapsulated in stiff hydrogels over the three-day experiment in atmospheric and hypoxic conditions. (**C**) Quantification of the percentage of apoptotic cells (sub-$G_1$) in the various conditions. (**Di, ii**) Quantitative RT-PCR for BNIP3 and GLUT-1 expression in HT1080 cells encapsulated in hydrogels of medium stiffness (3D) and in Petri dishes (plates) in atmospheric and hypoxic conditions. Significance levels (n=3) were set at: *p<0.05, **p<0.01, and ***p<0.001.

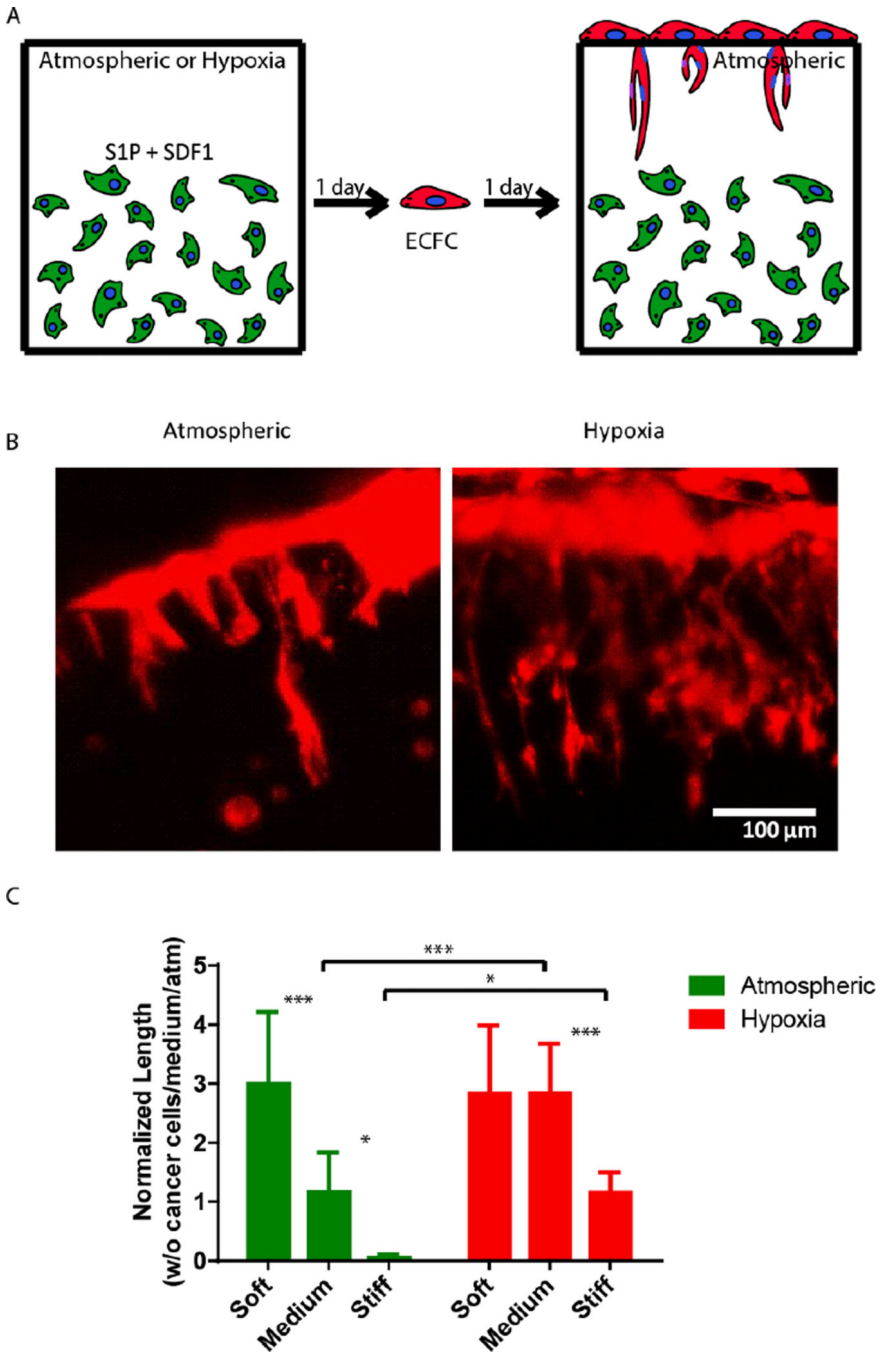


**Figure 5. Effect of AHA-HT1080 on ECFC sprouting and invasion**

(**A**) Schematic of study strategy for examining the angiogenic potential of AHA-HT1080 constructs: HT1080 cells, SDF1α, and S1P were encapsulated in AHA hydrogels of different stiffnesses and cultured for 24 hours in hypoxic or atmospheric conditions, followed by seeding of ECFCs as a monolayer on top of the hydrogels and culturing for an additional 24 hours. (**B**) Lectin stain (in red) and side-view imaging of endothelial sprouting in medium hydrogel in atmospheric and hypoxic conditions. (**C**) Quantification of sprouting

length of ECFCs in the different stiffness and oxygen tension conditions. Significance levels (n=3) were set at: *p<0.05, **p<0.01, and ***p<0.001.

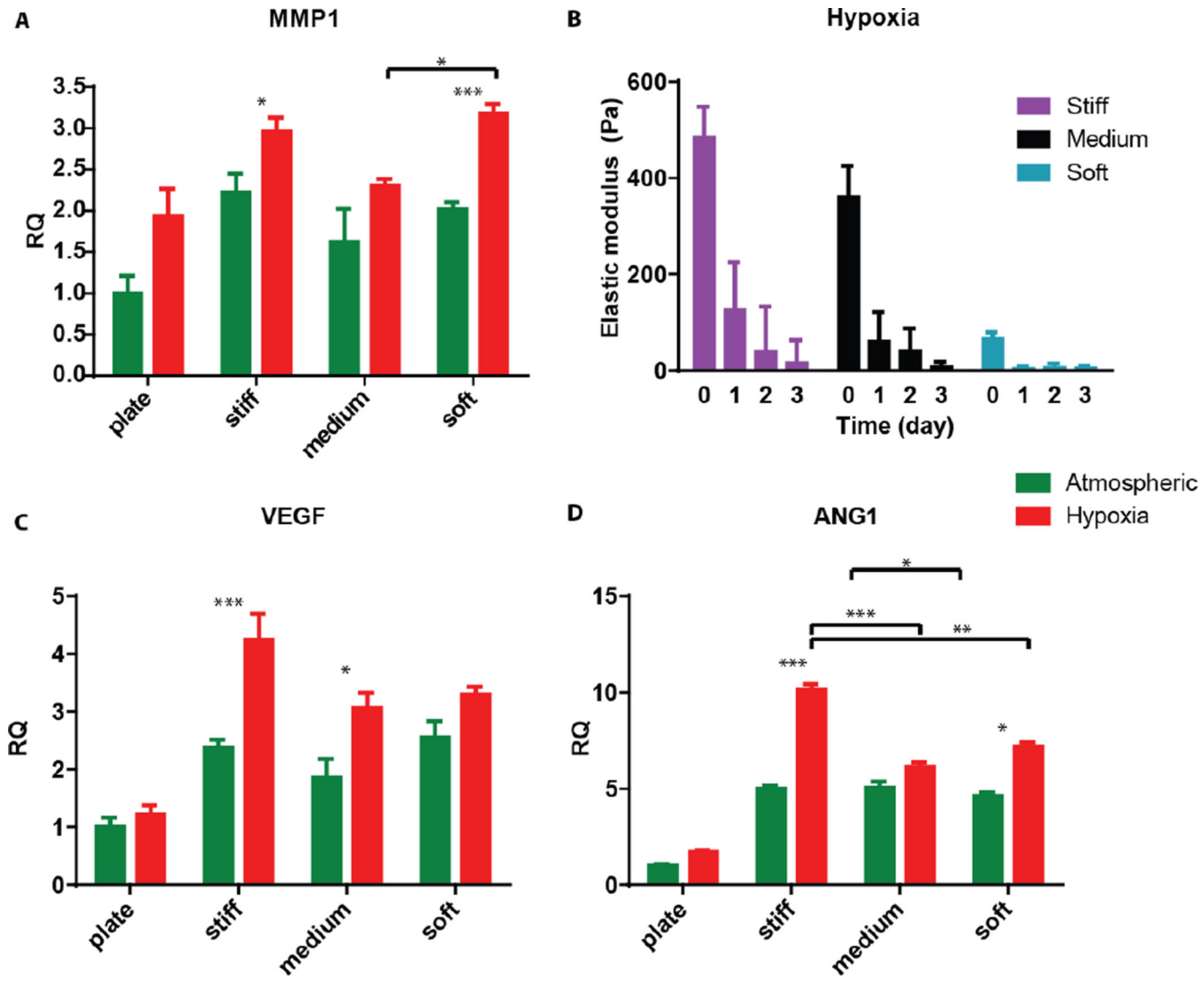


**Figure 6. Angiogenic gene expression**

(**A**) Quantitative RT-PCR for the expression of MMP-1 in HT1080 cells cultured in Petri dishes (plates) or encapsulated in the different hydrogels for 24 hours. (**B**) Viscoelasticity measurements of the different construct types along the three-day hypoxic culture period. (**D**-**C**) Quantitative RT-PCR for the expression of VEGF, and ANG-1 in HT1080 cells cultured in Petri dishes (plates) or encapsulated in the different hydrogels for 24 hours. Significance levels (n=3) were set at: *p<0.05, **p<0.01, and ***p<0.001.